

PAPER • OPEN ACCESS

# Design of quasi-axisymmetric stellarators with varying-thickness permanent magnets based on Fourier and surface magnetic charges method

To cite this article: G.S. Xu *et al* 2021 *Nucl. Fusion* **61** 026025

View the [article online](#) for updates and enhancements.

You may also like

- [Electrodynamics in cylindrical symmetry in the magnetic plasma state](#)  
F I López-Bara and F López-Aguilar
- [Theoretical analyses of magnetoelectric effects for magnetostrictive/radial mode piezoelectric transformer composite under dual ac stress and magnetic field modulation](#)  
Ning Xiao, Yao Wang, Lei Chen et al.
- [Design of quasi-axisymmetric stellarators with variable-thickness perpendicular permanent magnets based on a two-step magnet design strategy](#)  
Z.Y. Lu, G.S. Xu, D.H. Chen et al.

# Design of quasi-axisymmetric stellarators with varying-thickness permanent magnets based on Fourier and surface magnetic charges method

G.S. Xu<sup>1,\*</sup>, Z.Y. Lu<sup>1,2</sup>, D.H. Chen<sup>1,\*</sup>, L. Chen<sup>1</sup>, X.Y. Zhang<sup>1,2</sup>, X.Q. Wu<sup>1</sup>, M.Y. Ye<sup>2</sup> and B.N. Wan<sup>1</sup>

<sup>1</sup> Institute of Plasma Physics, Hefei Institutes of Physical Science, Chinese Academy of Sciences, Hefei 230031, China

<sup>2</sup> University of Science and Technology of China, Hefei 230026, China

E-mail: [gsxu@ipp.ac.cn](mailto:gsxu@ipp.ac.cn) and [dehong.chen@ipp.ac.cn](mailto:dehong.chen@ipp.ac.cn)

Received 17 September 2020, revised 5 November 2020

Accepted for publication 25 November 2020

Published 14 January 2021



CrossMark

## Abstract

To obtain engineering-feasible designs of stellarators with permanent magnets and simplified coils, a new algorithm has been developed based on Fourier decomposition and surface magnetic charges method. The strong toroidal fields in a quasi-axisymmetric stellarator are still generated by coils. The permanent magnets are designed to compensate the normal magnetic field  $B_n$  on the plasma surface  $\partial P$  created by the coils and plasma. The normal magnetic fields created by the permanent magnets  $B_{pmn}$  are calculated as the difference between the magnetic fields created by the surface magnetic charges on the inner surface  $\partial D$  and the outer surface  $\partial D_n$  of the magnets. The Fourier coefficients of the magnet thickness function  $h(\theta, \phi)$  are computed through matrix division operation based on the least square principle with dominant Fourier components selected through 2D Fourier transformation of  $B_{pmn}$ . The residual uncompensated  $B_n$  is minimized through iteration to progressively optimize the thickness function. This new algorithm has been successfully applied to design the permanent magnets of an  $l = 2$  quasi-axisymmetric stellarator with background magnetic field created by 12 identical circular planar coils for demonstrations. High accuracy has been achieved, allowing for a flux-surface-averaged residual  $B_n$  relative to the total field  $\langle |B_n/B| \rangle \sim 1.3 \times 10^{-5}$  and a maximum residual  $B_n$  of less than 2 Gs for  $\sim 1$  T total field. This new design has some advantages in engineering implementations: all permanent magnet pieces have the same remanence  $B_r$ ; only one single layer of magnets are mounted perpendicular to the winding surface; the magnets can be easily inserted into the cells of a gridded frame attached to the winding surface and fixed with springs from the back, which greatly simplifies the manufacture, assembly and maintenance of the magnets, and thus facilitates precision control and cost reduction.

\* Authors to whom any correspondence should be addressed.



Original content from this work may be used under the terms of the [Creative Commons Attribution 3.0 licence](https://creativecommons.org/licenses/by/3.0/). Any further distribution of this work must maintain attribution to the author(s) and the title of the work, journal citation and DOI.

Keywords: quasi-axisymmetric stellarator, permanent magnet, optimization algorithm, Fourier decomposition, coil design, surface magnetic charges

(Some figures may appear in colour only in the online journal)

## 1. Introduction

Intrinsically steady-state operation, nearly disruption-free and low recirculating power make stellarator an attractive fusion reactor candidate [1]. Historically, stellarators lagged behind tokamaks due to their relatively poor neoclassical confinement. To improve the neoclassical confinement, quasi-symmetry was introduced into the stellarator optimization and the effect has been demonstrated in the HSX stellarator experiments [2]. Recently, the remarkable success of the W7-X stellarator shows that neoclassical optimization can improve the confinement of stellarators up to a level similar to tokamaks [3]. The conventional stellarators use external coils to produce a non-axisymmetric magnetic field which confines the plasma and create the required rotational transform. The required coils in a stellarator are thus very complicated and contribute significantly to the overall cost of the device [4]. Coil complexity is one of the main challenges for stellarators. Modern stellarators use discrete modular coils instead of continuous coils. Even with optimized modular coils, difficulties in fabrication and assembly of the complex 3D non-planar coils with required accuracy and the anticipated strong mechanical stresses in the coils and the support structure of the coils for a reactor-size device have been the main challenges for the development of the stellarator approach as a fusion reactor candidate [5].

Recent study suggests that permanent magnets can be used to create rotational transform in a stellarator, thus substantially simplifying the coils [6], which may facilitates machine construction and cost reduction. More important, higher field strength can be achieved for a reactor-size stellarator as the mechanical stresses in the coils and the support structure of the coils are reduced. Identical planar coils with circular cross-section have been proven sufficient for a quasi-axisymmetric stellarator, leaving permanent magnets to do most of the plasma shaping. The strong background toroidal magnetic fields in a quasi-axisymmetric stellarator are still generated by coils. The permanent magnets can be used just to compensate the fields perpendicular to the plasma outermost surface, i.e., the last closed flux surface. Therefore, the required field strength created by the permanent magnets is not so strong (typically  $<0.5$  T) for an experimental device without blanket or with a thin blanket ( $<0.3$  m). Such field strength is achievable with commercially available permanent magnets which have a remanence of  $B_r \leq 1.55$  T [7]. In contrast to coils, permanent magnets can provide a steady magnetic field without energy

consumption, be arranged in complicated patterns, and more importantly, the materials are relatively inexpensive compared with superconducting materials, thus may drastically reduce the capital cost of a stellarator. However, compared with superconducting magnets the disadvantage is that the magnetic field strength produced by permanent magnets cannot change once the device has been assembled.

Several algorithms have been proposed recently for the design of permanent magnets and applied to the design of quasi-axisymmetric stellarators with highly simplified coils. One is to design the distribution and orientation of the magnetization  $\mathbf{M}$  of permanent magnets with a fixed thickness [6]. This work verifies the feasibility of creation of rotational transform in a stellarator using permanent magnets. With spatially varying magnetization, engineering realization is difficult as the magnets need to be magnetized to different remanence, which would dramatically increase the difficulty in magnetization precision control and the manufacturing cost. An improved algorithm, the so-called ‘multi-layer method’, has been explored, through varying the thickness of permanent magnets perpendicular to the installation surface, i.e., the ‘winding surface’, with a fixed magnetization  $M$  [8]. This algorithm calculates the distribution of one thin layer (1 mm thick) of permanent magnets for each step, and then iterates through incrementally stacking magnets layer by layer from innermost to outermost surface with linear method based on the surface current potential distributions, so that the existing codes for stellarator coil design can be used for the permanent magnet design. The solution with this algorithm provides a good initial guess for further optimizations. Recently, a more sophisticated algorithm has been proposed based on finite elements of discretized magnetic dipole moments [9] using the so-called ‘density method’ [10] with a penalization technique which employs a continuous exponential function to penalize the intermediate values between 0 and 1 to achieve a polarized distribution of the magnet normalized density  $\rho$ . With this algorithm, the restriction on the magnetic-dipole orientations can be relaxed, so that the so-called ‘Halbach’ arrays [11] are formed and less magnets are used than the linear method. In addition, it allows to reserve space for ports, showing attractively large access on the outboard side. More recently, a preliminary study of geometric concepts for magnet arrays is performed [12]. Two classes of magnet geometry, curved bricks and hexahedra, are explored.

Engineering implementation favors uniform remanence and simple geometry for all magnet pieces and a relatively small

number of magnet pieces, to simplify the manufacture, assembly and maintenance of the magnets, and reduce the cost. If each magnet piece is too small, there will be a huge number of pieces, which may lead to assembly errors and accumulated errors in the produced magnetic field. Thus, it is worth seeking more advanced algorithms for engineeringly practical magnet design. In this paper a new algorithm is proposed with fixed remanence  $B_r$  and varying magnet thickness perpendicular to the installation surface based on Fourier decomposition and surface magnetic charges method, which has been demonstrated to be a very effective algorithm, capable of achieving the design targets with high accuracy and a relatively small number of magnet pieces, thus exhibiting attractive engineering feasibility.

This paper is organized as follows. In section 2, the new algorithm and its design logic are introduced with formulations. In section 3, application of this new algorithm to an  $l = 2$  quasi-axisymmetric stellarator with a  $\beta = 0$  equilibrium is presented. In section 4, numerical validations with field-line tracing are carried out to check the accuracy of the produced flux surfaces relative to the equilibrium flux surfaces. A summary and discussions for future application and development are presented in the last section.

## 2. Algorithm

To introduce the new algorithm with illustrations, a  $\beta = 0$  equilibrium for ESTELL stellarator [13] is used, which is an optimized two-period  $l = 2$  quasi-symmetric stellarator with average major radius of the magnetic axis  $R_0 = 1.3944$  m and average field strength on the magnetic axis  $B_0 = 1$  T. It was originally obtained by deforming a classical  $l = 2$  stellarator with aspect ratio  $A = 5$  into a shape that makes the magnetic field quasi-axisymmetric. This means that the field strength is nearly independent of the toroidal angle in Boozer or Hamada coordinates, which ensures good orbit confinement [14–16]. Here,  $\beta = 0$  implies that there is no magnetic field produced by plasma current,  $B_{\text{plasma}} = 0$ . Figure 1 shows the permanent magnet distribution designed for this ESTELL equilibrium.

The permanent magnets are composed of 120 (poloidal)  $\times$  240 (toroidal) small pieces, mounted on the winding surface  $\partial D$  with their magnetic axes perpendicular to this surface.  $\partial D$  could be the outer surface of the vacuum-chamber wall, which encloses and is at a distance  $d$  from the plasma surface  $\partial P$ .  $\partial D_h$  is the outer surface composed by the permanent magnets. This design greatly facilitates engineering assembly. The permanent magnets can be easily inserted into the cells of a gridded frame attached to the winding surface and fixed with springs and caps from the back as shown in figure 2. The distance between the winding surface  $\partial D$  and the plasma surface  $\partial P$  is  $d = 10$  cm and the maximum magnet thickness is  $h_{\text{max}} = 17.22$  cm in this example.

### 2.1. Magnetic field calculation using the surface magnetic charges method

We need to calculate the normal magnetic field component on the plasma surface generated by permanent magnets  $B_{\text{pmn}}$ .

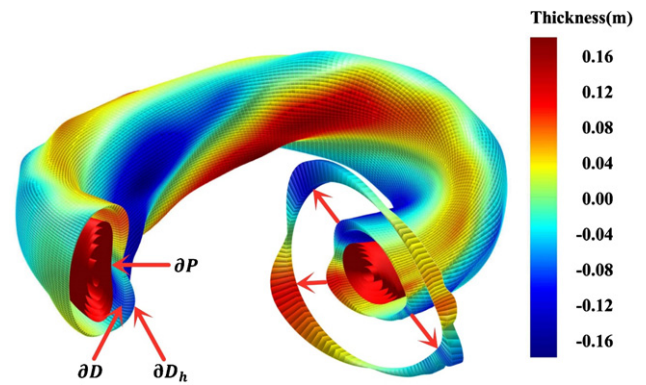


**Figure 1.** Permanent magnet distribution designed for a two-period  $l = 2$  quasi-axisymmetric stellarator with 120 (poloidal)  $\times$  240 (toroidal) pieces mounted on the winding surface  $\partial D$  with their magnetic axes perpendicular to this surface. The red flux surfaces show the area of plasma. The colorbar indicates the magnet thickness  $h$ , i.e., the distance between  $\partial D$  and  $\partial D_h$ . Positive value (red) means that the magnetic axis of the permanent magnet points away from the plasma and negative value (blue) means toward the plasma.

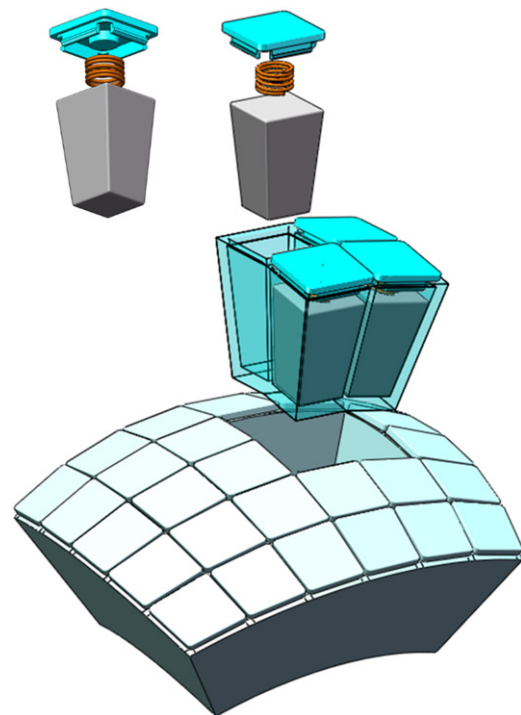


**Figure 2.** Schematic diagram of the concept for permanent magnet assembly. Magnet pieces are inserted into the cells of a gridded frame attached to the winding surface, fixed with springs and caps from the back.

The magnetic field generated by a piece of permanent magnet is governed by the Biot–Savart law. There are three methods to calculate the magnetic field, i.e., surface magnetic charges, effective currents and discretized magnetic dipoles. The method adopted in this paper is the surface magnetic charges [17], where the permanent magnets are modeled as distributed positive and negative magnetic monopoles with surface charges concentrating on the inner and outer surfaces

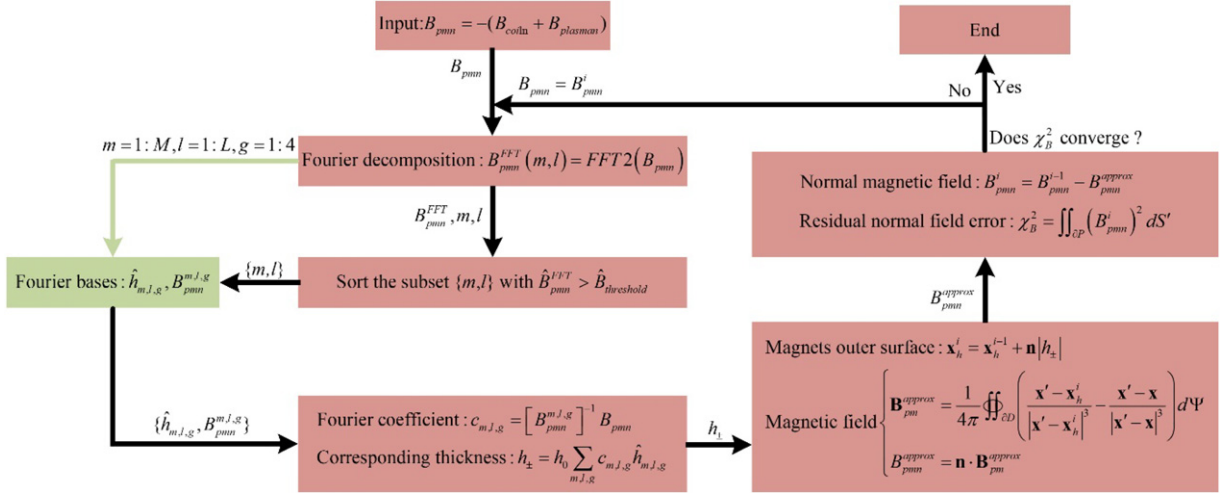


**Figure 3.** The iteration flow chart of the algorithm. The green part is a database of 2D Fourier base functions, which only needs to be calculated once. The red part is the iteration flow, which uses the database and upgrade the database if additional high-order Fourier base functions are needed.

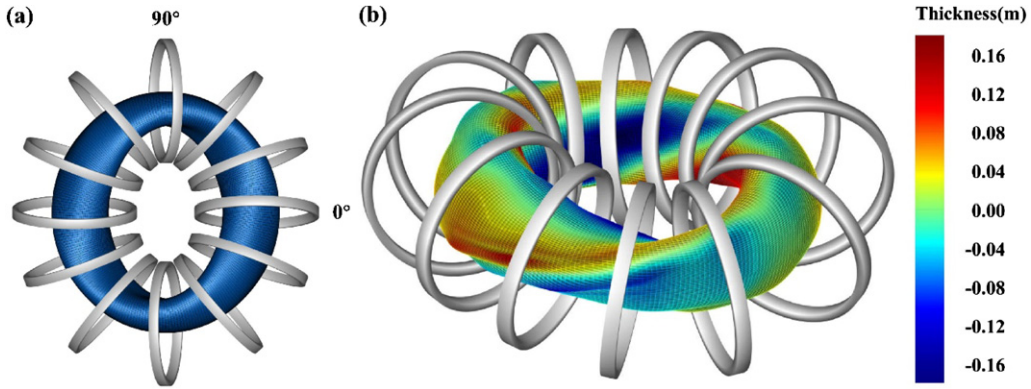


**Figure 4.** (a) The winding surface (blue) of a  $\beta = 0$  equilibrium for ESTELL, a two-period  $l = 2$  quasi-symmetric stellarator, shown with 12 identical circular cross-section planar coils, all carrying the same current 4.4116 kA. Each coil has  $15 \times 9$  turns. (b) The outer surface of the permanent magnets with color indicating the thickness.

of the permanent magnets situated ‘ $h$ ’ distance apart. The field strength at a field point  $\mathbf{x}' (x', y', z')$  on the plasma surface  $\partial P$  is a 2D integral across the winding surface  $\partial D$ ,

$$\mathbf{B} = \frac{1}{4\pi} \iint_{\partial D} \left( \frac{\mathbf{r}_h}{r_h^3} - \frac{\mathbf{r}}{r^3} \right) d\Psi \quad (1)$$

Hereafter, primes are used to denote coordinates on the plasma surface and un-primed for the winding surface.

Here,  $\mathbf{r} = \mathbf{x}' - \mathbf{x}$  is the position vector pointing from the source point on the winding surface  $\partial D$  to the field point and  $\mathbf{r}_h = \mathbf{x}' - \mathbf{x}_h$  is the position vector pointing from the source point on the outer surface of the permanent magnets  $\partial D_h$  to the field point.  $r = |\mathbf{r}|$  and  $r_h = |\mathbf{r}_h|$  are the corresponding distances.  $\mathbf{x} (x, y, z)$  is the source point on the winding surface  $\partial D$  and  $\mathbf{x}_h (x_h, y_h, z_h)$  is the source point on the outer surface of the permanent magnets  $\partial D_h$ , which is calculated with the coordinate relationship  $\mathbf{x}_h = \mathbf{x} + h\mathbf{n}$ , where  $\mathbf{n}$  is the unit normal vector of the winding surface with positive direction pointing outwards (away from the plasma).  $d\Psi = B_{r\pm} dS$  is the magnetic flux passing through the inner surface of a magnet piece,

i.e., a small quadrilateral on the winding surface.  $dS$  is its surface area, which is computed numerically from the coordinates of the quadrilateral’s four vertices.  $B_{r\pm}$  is the surface density of the surface magnetic charges. As the magnets are installed perpendicular to the winding surface,  $B_{r\pm}$  is also the normal field produced by the magnets on the winding surface,

$$B_{r\pm} = \mu_0 \mathbf{n} \cdot \mathbf{M} = B_r \text{sign}(\mathbf{n} \cdot \mathbf{M}) \quad (2)$$

where  $\text{sign}(\dots)$  is the sign function.  $B_{r\pm}$  is positive when the magnetization  $\mathbf{M}$  of the permanent magnet points outwards, i.e., away from the plasma. Its absolute value is equal to the remanence,  $|B_{r\pm}| = B_r$ . The remanence varies with materials and material grades. In this paper, we choose  $B_r = 1.4$  T for all the calculations, as this is one of the most widely commercially available neodymium–iron–boron (Nd–Fe–B) magnet at room temperature in the market [7]. Note that here it has been assumed that the magnetic flux passing through the outer surface of the permanent magnets is approximately equal to that passing through the inner surface, since there are nearly no gaps between adjacent magnets.

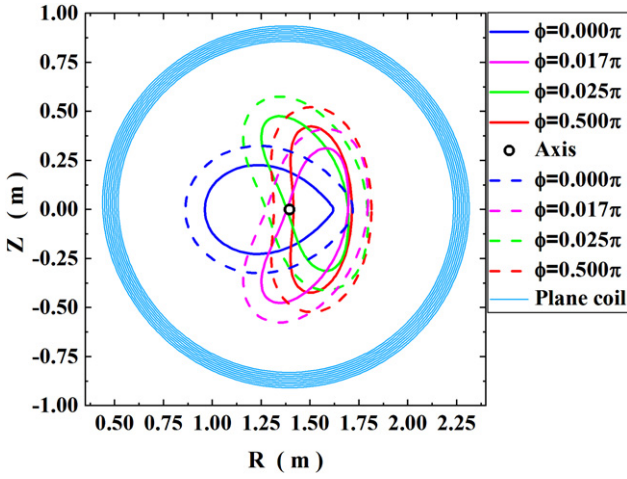


**Figure 5.** Cross sections of plasma surface (solid curves) and winding surface (dashed curves) at 4 toroidal locations. Projection of the coil at  $\phi = 0^\circ$  (skyblue circles). Toroidally averaged magnetic axis (black hollow dot).

## 2.2. Design logic

**2.2.1. Coil design and optimization target.** Most of the magnetic fields in a quasi-axisymmetric stellarator are toroidal magnetic fields which are still produced by coils. Identical circular cross-section planar coils are used to generate the background magnetic field  $\mathbf{B}_{\text{coil}}$  (mostly toroidal field) with the minimum field strength (near the outer midplane) equal to that of the equilibrium field strength,  $B_{\text{coil min}} = B_{\text{eq min}}$ , to minimize the magnet coverage and offer large access to the plasma on the outboard side, which can be used for heating systems, diagnostics and remote maintenance. The easy access for remote maintenance is extremely favourable for future fusion reactors. The magnetic field component normal to the plasma surface generated by the coils is  $B_{\text{coiln}} = \mathbf{B}_{\text{coil}} \cdot \mathbf{n}'$ , where  $\mathbf{n}'$  is the unit normal vector of the plasma surface with positive direction pointing outwards (away from the plasma). The total equilibrium magnetic field consists of three components,  $\mathbf{B}_{\text{eq}} = \mathbf{B}_{\text{coil}} + \mathbf{B}_{\text{pm}} + \mathbf{B}_{\text{plasma}}$ . Since there is no magnetic field produced by plasma current in this case,  $\mathbf{B}_{\text{plasma}} = 0$ , the magnetic field needs to be produced by the permanent magnets is  $\mathbf{B}_{\text{pm}} = \mathbf{B}_{\text{eq}} - \mathbf{B}_{\text{coil}}$ .

The permanent magnets are designed to compensate the normal fields produced by the coils and plasma on the plasma surface,  $B_{\text{pmn}} = \mathbf{B}_{\text{pm}} \cdot \mathbf{n}' = -B_{\text{coiln}} - B_{\text{plasma}}$ , so as to minimize the surface integral of the residual normal field square, the so-called residual normal field error,

$$\chi_B^2 = \iint_{\partial P} B_n^2 dS' \quad (3)$$

where  $B_n = B_{\text{coiln}} + B_{\text{pmn}}^{\text{approx}} + B_{\text{plasma}}$  is the residual normal field on the plasma surface, which progressively vanishes through iteration, so that  $\chi_B^2 \rightarrow 0$ . Here,  $B_{\text{pmn}}^{\text{approx}}$  is produced by the permanent magnets, which approximates the compensation target,  $B_{\text{pmn}}^{\text{approx}} \approx B_{\text{pmn}}$ .

Figure 3 outlines the algorithm. After coil design, a database of 2D Fourier base functions is built, as shown in

the green part of figure 3, introduced in subsection 2.2.4. The database only needs to be calculated once. Then, iteration starts until a convergence criterion is reached. The iteration flow is shown in the red part of figure 3, which will be introduced step by step in the following subsections.

**2.2.2. 2D Fourier transformation of normal field on the plasma surface.** A magnetic-flux coordinate system  $(\theta, \phi, \psi)$  is used with grids 120 (poloidal)  $\times$  240 (toroidal)  $\times$  65 (radial). Here,  $\theta$ ,  $\phi$  and  $\psi$  are the poloidal angle, toroidal angle and magnetic flux surface coordinates, respectively. For the flux surface coordinate  $\psi$ , the first layer is the magnetic axis and the outermost layer (65) is the plasma surface. Note that some calculations in this algorithm are performed in the Cartesian coordinate system  $(x, y, z)$ . A transformation connects these two coordinate systems.

We find that the normal field  $B_{\text{pmn}}(\theta, \phi)$  is a 2D continuous function. Its 2D Fourier transformation is calculated,

$$B_{\text{pmn}}^{\text{FFT}}(m, l) = \text{FFT}_2 [B_{\text{pmn}}(\theta, \phi)] \quad (4)$$

and normalized to its maximum,  $\hat{B}_{\text{pmn}}^{\text{FFT}} = B_{\text{pmn}}^{\text{FFT}} / \max(B_{\text{pmn}}^{\text{FFT}})$ . Here,  $m$  is the poloidal mode number and  $l$  is the toroidal mode number. Next, a threshold is used to find out the dominant Fourier components,

$$\hat{B}_{\text{pmn}}^{\text{FFT}} > \hat{B}_{\text{threshold}} \quad (5)$$

Only these Fourier components are compensated by the magnetic field generated by the permanent magnets. The other Fourier components are neglected as their amplitudes are small. This spectral truncation method effectively saves computing resources. The NESCOIL code developed by Merkel also uses the spectral truncation method to represent the surface current potential  $\Phi$  in the design of stellarator coils [18].

**2.2.3. 2D Fourier expansion of thickness function on the winding surface.** The distributions of magnet thickness and orientation (toward or away from the plasma) on the winding surface are 2D functions,  $h(\theta, \phi)$  and  $\text{sign}[B_{\text{r}\pm}(\theta, \phi)]$ . Here,  $B_{\text{r}\pm}(\theta, \phi)$  is the normal field generated by permanent magnets on the winding surface. We introduce a thickness function to describe both the distribution and orientation of the permanent magnets.

$$h_{\pm}(\theta, \phi) \equiv h(\theta, \phi) \text{sign}[B_{\text{r}\pm}(\theta, \phi)] \quad (6)$$

Note that  $h_{\pm}(\theta, \phi)$  is a signed function. Since in this design the permanent magnets are mounted perpendicular to the winding surface, also nearly perpendicular to the plasma surface, and the winding surface is very close to the plasma surface,  $h_{\pm}(\theta, \phi)$  has a 2D distribution pattern similar to  $B_{\text{pmn}}(\theta, \phi)$ . Therefore, the dominant Fourier components in  $B_{\text{pmn}}(\theta, \phi)$  are also the ones in  $h_{\pm}(\theta, \phi)$ . The 2D Fourier expansion of  $h_{\pm}(\theta, \phi)$  can be written as,

$$h_{\pm}(\theta, \phi) = h_0 \sum_{m,l,g} c_{m,l,g} \hat{h}_{m,l,g}(\theta, \phi) \quad (7)$$

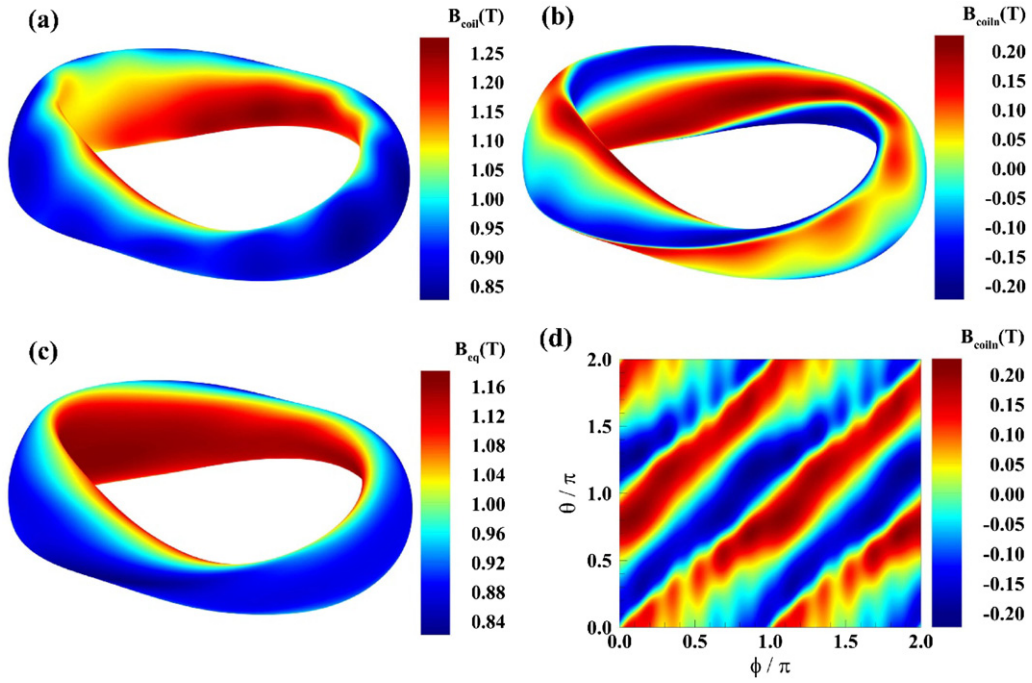


**Figure 6.** Magnetic fields on the plasma surface, (a) total magnetic field generated by coils  $B_{\text{coil}}$ , (c) total equilibrium magnetic field  $B_{\text{eq}}$ , (b) 3D plot and (d) contour plot of the normal field produced by the coils  $B_{\text{coiln}}$ .

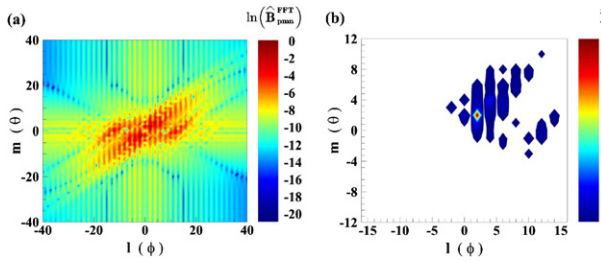


**Figure 7.** (a) 2D spectrum of the normal field on the plasma surface with natural logarithm of the normalized amplitude  $\ln(\hat{B}_{\text{pmn}}^{\text{FFT}})$ , (b) 2D spectrum with the normalized amplitude above a threshold  $\hat{B}_{\text{threshold}} = 0.01$ . In order to reduce computational cost, for those Fourier modes with the same  $|m|$  and  $|l|$  numbers, only one mode is left.

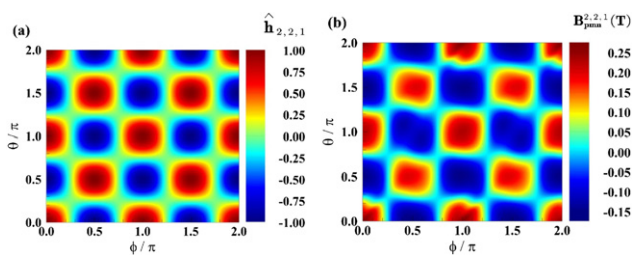


**Figure 8.** Contour plots of (a) the 2D Fourier base function  $\hat{h}_{2,2,1}(\theta, \phi)$  for the largest Fourier component  $m, l = 2, 2$  and (b) the normal field on the plasma surface  $B_{\text{pmn}}^{2,2,1}(\theta, \phi)$  produced by the corresponding permanent magnets.

where  $h_0 = 0.1m$  is a constant,  $c_{m,l,g}$  are the Fourier coefficients and  $\hat{h}_{m,l,g}(\theta, \phi)$  are the 2D Fourier base functions. The thickness and orientation can be calculated from  $h_{\pm}(\theta, \phi)$ , i.e.,  $h(\theta, \phi) = |h_{\pm}(\theta, \phi)|$  and  $B_{\pm}(\theta, \phi) = B_r \text{sign}[h_{\pm}(\theta, \phi)]$ .

The 2D Fourier base functions  $\hat{h}_{m,l,g}(\theta, \phi)$  have four kinds of combinations:  $\hat{h}_{m,l,1}(\theta, \phi) = \cos(m\theta) \cos(l\phi)$ ,  $\hat{h}_{m,l,2}(\theta, \phi) = \cos(m\theta) \sin(l\phi)$ ,  $\hat{h}_{m,l,3}(\theta, \phi) = \sin(m\theta) \cos(l\phi)$  and  $\hat{h}_{m,l,4}(\theta, \phi) = \sin(m\theta) \sin(l\phi)$ . Note that there are some Fourier base functions equal to zero for  $\sin(\dots) = 0$  when  $m = 0$  or  $l = 0$ . Now, the problem translates into calculating the Fourier coefficients,  $c_{m,l,g}$ . Because of the truncation of Fourier series, the magnetic field will inevitably lose some details with the finite Fourier modes. This is an ill-posed inverse problem, which can be solved using matrix division operation based on the least square principle [19].

**2.2.4. Build a database of 2D Fourier base functions.** The normal fields on the plasma surface  $B_{\text{pmn}}^{m,l,g}(\theta, \phi)$  produced by the permanent magnets with each Fourier component of the thickness distribution  $h_{m,l,g}(\theta, \phi) = h_0 |\hat{h}_{m,l,g}(\theta, \phi)|$  and orientation distribution  $B_{\text{r}\pm}^{m,l,g}(\theta, \phi) = B_r \text{sign}[\hat{h}_{m,l,g}(\theta, \phi)]$  described by the 2D Fourier base functions  $\hat{h}_{m,l,g}(\theta, \phi)$  are calculated in advance, constituting a database for  $m = 0 : M$ ,  $l = 0 : L$  and  $g = 1 : 4$ . Only nonzero Fourier base functions  $\hat{h}_{m,l,g}(\theta, \phi)$  are included in the database. It is found that a database with  $M = 16$  and  $L = 42$  can provide sufficient precision for the following optimization. In the code, for each time iteration, if a Fourier mode outside the database appears, i.e.,  $m > M$  or  $l > L$ , the corresponding data of this Fourier mode, including the normal fields on the plasma surface  $B_{\text{pmn}}^{m,l,g}(\theta, \phi)$ , will be calculated and added into the database to update the database. When the iteration ends, if the database is almost unchanged, which means that most of the Fourier modes involved in the optimization process have been included in the database with the given selection criteria of Fourier mode, the database is considered to be big enough. The magnetic

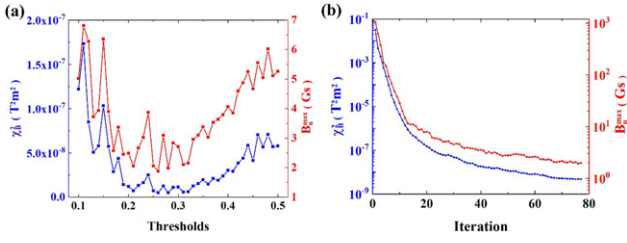


**Figure 9.** (a) Threshold  $\hat{B}_{\text{threshold}}$  scan to find out the best threshold with minimum residual normal field error  $\chi_B^2$ , shown in blue. The maximum of residual normal field on the plasma surface  $B_n^{\text{max}}$  is shown in red. (b) For the best threshold  $\hat{B}_{\text{threshold}} = 0.28$ ,  $\chi_B^2$  (blue) and  $B_n^{\text{max}}$  (red) converge to  $4.786 \times 10^{-9}$  and 1.986 Gs, respectively, after 77 times iterations.

field on the plasma surface  $\mathbf{B}_{\text{pmn}}^{m,l,g}(\theta, \phi)$  is calculated using the surface magnetic charges method according to equation (1) with the coordinate relationship  $\mathbf{x}_h = \mathbf{x} + \mathbf{n}h_{m,l,g}(\theta, \phi)$  and the magnetic flux  $d\Psi = B_{r\pm}^{m,l,g}(\theta, \phi) dS$ . Then, the normal field is obtained,  $B_{\text{pmn}}^{m,l,g}(\theta, \phi) = \mathbf{n} \cdot \mathbf{B}_{\text{pmn}}^{m,l,g}(\theta, \phi)$ .

**2.2.5. Calculations of Fourier coefficients and residual normal field.** For each iteration, the Fourier decomposition is conducted with the updated normal field on the plasma surface. A subset of Fourier modes  $\{m, l, g\}$  is picked out from the database of the 2D Fourier base functions with the selection criteria, in equation (5), and sorted out according to the normalized spectral amplitude. The parameter  $g = 1:4$  corresponds to four kinds of combinations, as given in the last paragraph of section 2.2.3. Then, the Fourier coefficients  $c_{m,l,g}$  are calculated through matrix division operation based on the least square principle [19],

$$c_{m,l,g} = [\mathbf{B}_{\text{pmn}}^{m,l,g}(\theta, \phi)]^{-1} B_{\text{pmn}}(\theta, \phi) \quad (8)$$

where  $[\dots]^{-1}$  is the generalized inverse of a matrix. The magnet thickness function  $h_{\pm}(\theta, \phi)$  is constructed from the Fourier components by following equation (7). Then, we have the thickness  $h(\theta, \phi)$  and orientation  $B_{r\pm}(\theta, \phi)$ . The magnetic field on the plasma surface  $\mathbf{B}_{\text{pmn}}^{\text{approx}}(\theta, \phi)$  produced by these permanent magnets is calculated using the surface magnetic charges method according to equation (1) with the coordinate relationship  $\mathbf{x}_h = \mathbf{x} + \mathbf{n}h(\theta, \phi)$  and magnetic flux  $d\Psi = B_{r\pm}(\theta, \phi) dS$ . Finally, we obtain the approximate normal field on the plasma surface produced by the permanent magnets  $B_{\text{pmn}}^{\text{approx}}(\theta, \phi) = \mathbf{n} \cdot \mathbf{B}_{\text{pmn}}^{\text{approx}}(\theta, \phi)$  and the residual normal field  $B_{\text{pmn}}^{\text{residual}}(\theta, \phi) = B_{\text{pmn}}(\theta, \phi) - B_{\text{pmn}}^{\text{approx}}(\theta, \phi)$  which is the compensation target for the next iteration.

**2.2.6. Iteration to progressively correct the thickness function.** Iteration starts. The 2D Fourier transformation of  $B_{\text{pmn}}^{\text{residual}}(\theta, \phi)$  is calculated and the dominant Fourier components is obtained with the same threshold  $\hat{B}_{\text{threshold}}$ . A new subset  $\{m, l, g\}$  in the database of the 2D Fourier base functions is sorted out according to the dominant Fourier components. Then, a new set of Fourier coefficients are calculated through matrix division operation  $c_{m,l,g} = [\mathbf{B}_{\text{pmn}}^{m,l,g}(\theta, \phi)]^{-1} B_{\text{pmn}}^{\text{residual}}(\theta, \phi)$  based on the least square principle. With these Fourier coefficients, we obtain a correction to the magnet thickness function  $\Delta h_{\pm}(\theta, \phi)$

according to equation (7) and a corrected thickness function  $h_{\pm}^i(\theta, \phi) = h_{\pm}^{i-1}(\theta, \phi) + \Delta h_{\pm}^i(\theta, \phi)$ . Note that  $h_{\pm}(\theta, \phi)$  is still a signed function. Again,  $\mathbf{B}_{\text{pmn}}^{\text{approx}}(\theta, \phi)$  is calculated using the surface magnetic charges method.  $B_{\text{pmn}}^{\text{approx}}(\theta, \phi)$  and  $B_{\text{pmn}}^{\text{residual}}(\theta, \phi)$  are obtained as well. Next, we use the residual normal field on the plasma surface  $B_n(\theta, \phi) = B_{\text{coiln}}(\theta, \phi) + B_{\text{pmn}}^{\text{approx}}(\theta, \phi)$  to calculate the residual normal field error  $\chi_B^2$  according to equation (3). Eventually, the threshold  $\hat{B}_{\text{threshold}}$  is scanned, repeating the iteration, to find out the best threshold with minimum  $\chi_B^2$ . The iteration stops when a convergence criterion is reached, i.e.,  $\chi_B^2$  exceeds the average of the last 5  $\chi_B^2$  values. Then, the iteration with the minimum  $\chi_B^2$  is given as the final result. Under ideal condition,  $\chi_B^2$  will decrease all the way down and never increase between iterations. However, some fine structures associated with the high-order Fourier components of the normal field on the plasma surface are abandoned due to the truncation of the Fourier series. As approaching convergence, the optimization focuses on the fine structures,  $\chi_B^2$  thus fluctuates between iterations. The stopping condition used in this paper is equivalent to the last five-point average of  $\chi_B^2$  over iterations, which is thus insensitive to the fluctuations. Although tolerance can also be used as a stopping condition. However, if the default tolerance cannot be reached, the iteration will be stuck in an endless loop and wastes a lot of machine time. More important, it is difficult to find appropriate tolerances for different cases. The stopping condition used here can be applicable to most cases, provides good results with relatively few iterations and effectively avoids getting stuck in an endless loop.

### 3. Apply to an $I = 2$ quasi-axisymmetric stellarator

#### 3.1. Design of the circular planar coils

The first step is to design the coils. Since permanent magnets cannot create toroidal magnetic flux, coils are still necessary to generate a background magnetic field. The strongest magnetic field component in a quasi-axisymmetric stellarator is the toroidal field which is mainly created by coils. However, the utilization of permanent magnets substantially simplifies the coils. Only 12 identical circular cross-section planar coils are used with their coil planes perpendicular to the local magnetic axis, as shown in figure 4, so as to minimize the magnetic field created by permanent magnets, thus minimize the total usage of magnet material. Note that the magnetic axis is a closed 3D curve for a quasi-symmetric stellarator.

The coil centers have been shifted radially outward in the same coil planes by 0.12 m relative to the local magnetic axis to allow more space on the outboard side for easy access to the plasma and enough gaps between coils on the inboard side to avoid coil interacting with each other. The coil radius is set to 0.9 m to ensure that there is enough space between the coils and the winding surface for the assembly of permanent magnets, see figure 5. The distance between the plasma surface (solid curves) and the winding surface (dashed curves) keeps constant at  $d = 10$  cm.

Each coil has  $15 \times 9$  turns, carrying the same current  $I_{\text{coil}} = 4.4116$  kA. The magnetic field generated by the coils are

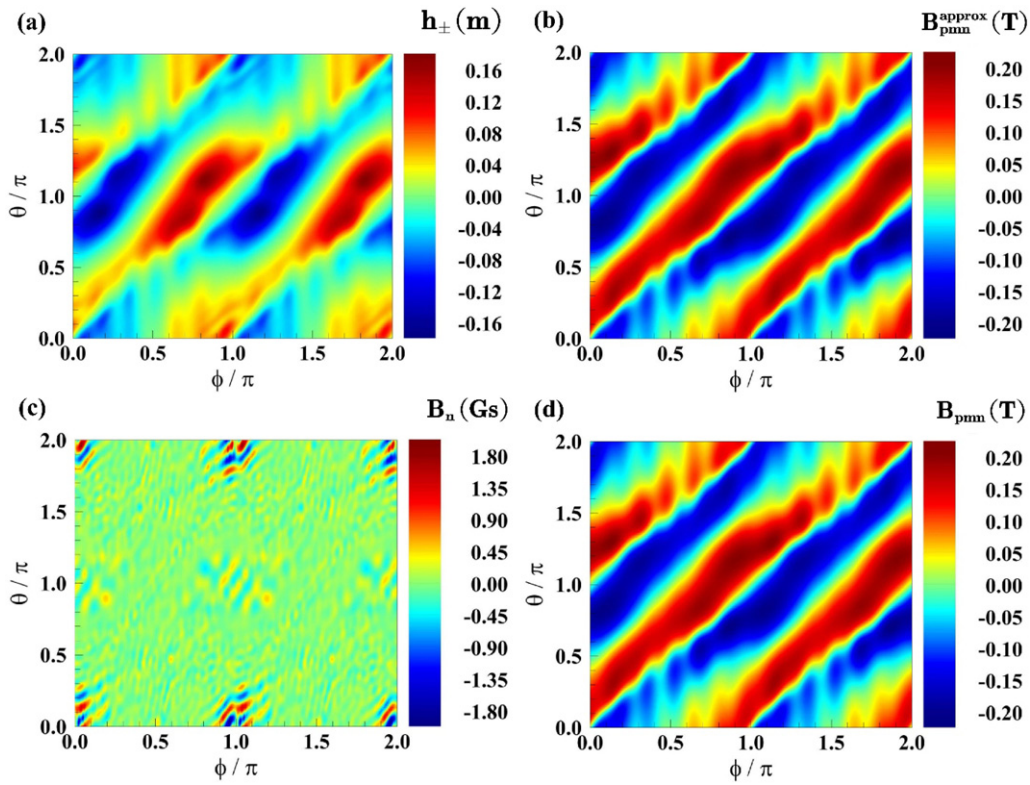


**Figure 10.** For the best threshold  $\hat{B}_{\text{threshold}} = 0.28$  after convergence, the contour plots of (a) the magnet thickness function  $h_{\pm}$ , (b) the normal field on the plasma surface produced by the permanent magnets  $B_{\text{pmn}}^{\text{approx}}$ , (c) the residual normal field on the plasma surface  $B_n = B_{\text{coiln}} + B_{\text{pmn}}^{\text{approx}}$  and (d) the normal field need to be produced by the permanent magnets  $B_{\text{pmn}} = -B_{\text{coiln}}$ .

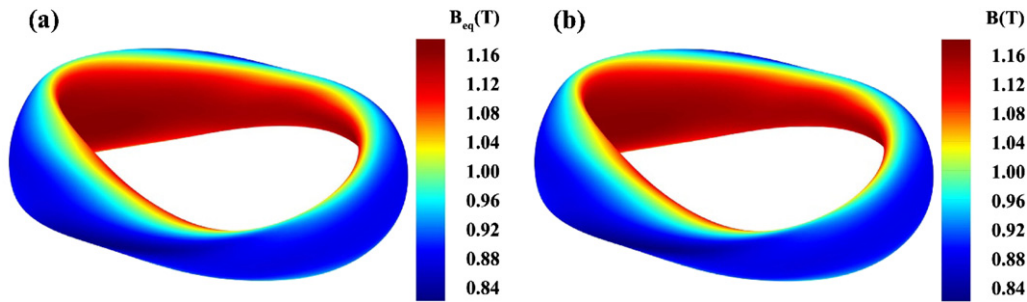


**Figure 11.** (a) The total equilibrium magnetic field  $B_{\text{eq}} = |\mathbf{B}_{\text{coil}} + \mathbf{B}_{\text{pmn}}|$  and (b) the total magnetic field  $B = |\mathbf{B}_{\text{coil}} + \mathbf{B}_{\text{pmn}}^{\text{approx}}|$  produced by the coils and permanent magnets on the plasma surface.

calculated by following the Biot–Savart law. The coil current is adjusted to match the minimum magnetic field strength (near the outer midplane) with that of the equilibrium magnetic field,  $B_{\text{coil min}} = B_{\text{min}} = 0.8213$  T. The maximum magnetic field on the inboard side is slightly stronger than that of the equilibrium magnetic field, as shown in figures 6(a) and (c). The differences need to be compensated by the magnetic field generated by permanent magnets.

The 3D plot and contour plot of the normal field produced by the coils  $B_{\text{coiln}}$  are shown in figures 6(b) and (d), respectively. The normal field needs to be produced by the permanent magnets is  $B_{\text{pmn}} = -B_{\text{coiln}}$ . The target is to calculate an approximate normal field  $B_{\text{pmn}}^{\text{approx}} \approx B_{\text{pmn}}$  to compensate the normal field produced by the coils  $B_{\text{coiln}}$  on the plasma surface

so that  $B_n = B_{\text{pmn}}^{\text{approx}} + B_{\text{coiln}}$  vanishes.  $B_{\text{pmn}}(\theta, \phi)$  appears to be a 2D continuous function. Its largest Fourier component is  $m, l = 2, 2$  mode and  $l = 12$  toroidal ripples can be clearly seen on the outboard side in figures 6(a), (b) and (d).

### 3.2. 2D Fourier transformation of the normal field on the plasma surface

In order to find out the dominant 2D Fourier components need to be produced by the permanent magnets, 2D Fourier transformation is applied to  $B_{\text{pmn}}(\theta, \phi)$ . There are many Fourier modes as shown in the 2D spectrum in figure 7(a), however, most of them have very small amplitude. Note that to enhance the spectral visibility natural logarithm has been used in figure 7(a),  $\ln(\hat{B}_{\text{pmn}}^{\text{FFT}})$ . The dominant Fourier components

are sorted out with a normalized-spectral-amplitude threshold,  $\hat{B}_{\text{pmn}}^{\text{FFT}} > \hat{B}_{\text{threshold}} = 0.01$ . The largest Fourier component appears to be  $m, l = 2, 2$  mode, as shown in figure 7(b).

### 3.3. Build a database of 2D Fourier base functions

The next step is to build a database of 2D Fourier base functions  $\hat{h}_{m,l,g}(\theta, \phi)$  and calculate the normal magnet field  $B_{\text{pmn}}^{m,l,g}(\theta, \phi)$  on the plasma surface produced by the permanent magnets described by the Fourier base functions. The largest Fourier component is  $m, l = 2, 2$ . The corresponding 2D Fourier base function  $\hat{h}_{2,2,1}(\theta, \phi)$  and normal field  $B_{\text{pmn}}^{2,2,1}(\theta, \phi)$  exhibit very similar distribution pattern, see figure 8. The similarity indicates that the Fourier expansion is an effective method in solving the inverse problem of permanent magnet design, similar to the NESCOIL code in designing the stellarator coils. We note that a deviations is visible in the distribution patterns between the two plots in figure 8, i.e., the magnet thickness pattern and the corresponding magnetic field pattern. It is not due to the mismatch in shape between the winding surface  $\partial D$  and the plasma surface  $\partial P$ , because the winding surface is generated through extending from the plasma surface along its normal vector with a fixed distance  $d$ , and thus they have the same shape. If the winding surface and the plasma surface are both planes and parallel to each other, there will be very little deviation. However, they are complicated three-dimensional surfaces with spatially varying surface curvatures. Therefore, the magnetic field pattern will be distorted relative to the magnet thickness pattern.

### 3.4. Iteration and convergence

Following the calculation steps introduced in section 2.2.5, we truncate a finite number of 2D Fourier components by setting a threshold to the spectral normalized amplitude,  $\hat{B}_{\text{pmn}}^{\text{FFT}} > \hat{B}_{\text{threshold}}$ , and calculate the Fourier coefficients  $c_{m,l,g}$  through matrix division operation based on the least square principle. Then, we obtain the approximate normal field on the plasma surface produced by the permanent magnets  $B_{\text{pmn}}^{\text{approx}}(\theta, \phi)$  and the residual normal field  $B_{\text{pmn}}^{\text{residual}}(\theta, \phi)$ . At this point, the first design cycle is complete. The initial maximum normal field on the plasma surface produced by the permanent magnets  $B_n^{\text{max}}$  ( $\sim 1000$  Gs) and the residual normal field error  $\chi_B^2$  ( $\sim 3 \times 10^{-2} \text{ T}^2 \text{ m}^2$ ) are still very large. They are effectively reduced through the iterations, as shown in figure 9(b).

Finally, the threshold  $\hat{B}_{\text{threshold}}$  is scanned from 0.1 to 0.5 as shown in figure 9(a). The best threshold with minimum residual normal field error  $\chi_B^2$  is found,  $\hat{B}_{\text{threshold}} = 0.28$ . With this threshold,  $\chi_B^2$  and the maximum of residual normal field on the plasma surface  $B_n^{\text{max}}$  converge to  $4.786 \times 10^{-9}$  and 1.986 Gs, reduced by 7 and 3 orders of magnitude, respectively, after 77 times iterations, as shown in figure 9(b).

The computation was performed using a computer workstation with 48 CPUs at 2.5 GHz. For spatial resolution 120 (poloidal)  $\times$  240 (toroidal) grids, each iteration needs roughly 16 min and the threshold scan from 0.1 to 0.5 with step 0.01 totally consumed  $\sim 8.1$  h. In addition, the 2D Fourier base function database calculation took  $\sim 7.1$  h, which only needs to be computed once.

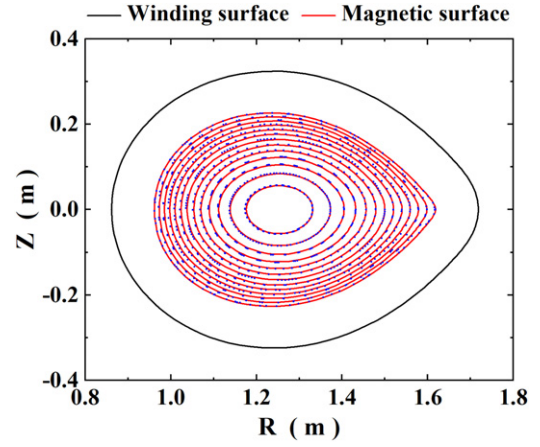


**Figure 12.** Poincaré plot on the plane at toroidal angle  $\phi = 0$  from field-line tracing in the magnetic field produced by the coils and permanent magnets  $\mathbf{B} = \mathbf{B}_{\text{coil}} + \mathbf{B}_{\text{pmn}}^{\text{approx}}$  is shown with blue dots. The cross-sections of equilibrium magnetic flux surfaces are shown with red curves. The winding surface is shown with a black curve. The field-line tracing appears to fit the equilibrium magnetic flux surfaces quite well.

With the best converged optimization results, the normal field on the plasma surface produced by the permanent magnets  $B_{\text{pmn}}^{\text{approx}}$  is a very good approximation to the normal field need to be produced by the permanent magnets  $B_{\text{pmn}} = -B_{\text{coiln}}$ , as shown in figures 10(b) and (d). Furthermore, the total magnetic field on the plasma surface produced by the coils and permanent magnets  $B = |\mathbf{B}_{\text{coil}} + \mathbf{B}_{\text{pmn}}^{\text{approx}}|$  is almost identical to the total equilibrium magnetic field  $B_{\text{eq}} = |\mathbf{B}_{\text{coil}} + \mathbf{B}_{\text{pm}}|$ , as shown in figure 11, which demonstrates the validity of the design algorithm. The residual normal field on the plasma surface  $|B_n| = |B_{\text{coiln}} + B_{\text{pmn}}^{\text{approx}}|$  is less than 2 Gs, see figure 10(c). The most uncompensated  $B_n$  mainly located near the outboard midplane around toroidal angle  $\phi = 0$  and  $\pi$ , where  $B_{\text{coiln}}$  has a sharp transition between positive and negative as shown in figure 6(b). More high order Fourier components are needed to compensate such sharp transition. This sets the lower limit of field-compensation and design accuracy for the Fourier based method. However, this location can be used to set up a divertor where finite  $B_n$  is favorable. The flux-surface-averaged residual normal fields relative to the total field on the plasma surface is  $\langle |B_n/B| \rangle \sim 1.3 \times 10^{-5}$ , exhibiting very high accuracy in the normal field compensation. In addition, the magnet thickness function  $h_{\pm}$  is shown in figure 10(a), which has a 2D distribution pattern very similar to  $B_{\text{pmn}}^{\text{approx}}$ , see figure 10(b). This leads us to come up with the idea of Fourier decomposition of the magnet thickness function.

## 4. Field line tracing to check the accuracy in generating the target equilibrium

Field-line tracing is calculated to check the accuracy of the produced magnetic flux surfaces relative to the equilibrium magnetic flux surfaces. Since a  $\beta = 0$  equilibrium has been used, there is no magnetic field produced by plasma current,

i.e.,  $B_{\text{plasma}} = 0$ , the total magnetic field is just the vacuum field, which is produced by the coils and permanent magnets  $\mathbf{B} = \mathbf{B}_{\text{coil}} + \mathbf{B}_{\text{pm}}^{\text{approx}}$ , and the Shafranov shift is zero as shown in figure 12. The field-line tracing results indicate that the vacuum flux surface fits the target equilibrium magnetic flux surfaces quite well. The relative difference of the rotational transform at the plasma surface (the last closed flux surface) is only  $\Delta t/t = 0.49\%$ , which verifies the validity of the design algorithm.

The field-line tracing is calculated in the Cartesian coordinate system with an improved six-order Runge–Kutta algorithm [20] following the field-line equation  $dB_x/dx = dB_y/dy = dB_z/dz$ . For each point on the tracing trajectory, the magnetic field is calculated based on the Biot–Savart law for the coils and the surface magnetic charges method for the permanent magnets.

## 5. Discussions and summary

By using permanent magnets, it has been proven possible to build optimized stellarators with extremely simple coils [6, 8, 9]. In this paper, a new algorithm has been proposed for the design of the permanent magnets. It mainly has three new features:

- (a) The surface magnetic charges method [17] has been introduced in this algorithm to calculate the magnetic field produced by the permanent magnets. Compared with other methods, such as the surface-current-potential method [8] and magnetic-dipole-moment method [9], this method is more suitable for the design of permanent magnets with varying thickness.
- (b) The permanent magnets are designed through progressively optimization of the thickness distribution with 2D Fourier decomposition of the thickness function. The Fourier components are selected according to a spectral amplitude truncation of the 2D Fourier transformation of the normal field on the plasma surface.
- (c) To solve the inverse problem, the Fourier coefficients of the magnet thickness function are computed through matrix division operation based on the least square principle [19].

For engineering implementations, this new design algorithm has several advantages:

- (a) All permanent magnet pieces have the same remanence  $B_r$ , which greatly simplifies the manufacture of the magnets, especially the magnetizing process and precision control. The cost is thus reduced.
- (b) Only one single layer of permanent magnets is installed perpendicular to the winding surface, which greatly simplifies the assembly process and maintenance. The permanent magnets can be easily inserted into the cells of a gridded frame attached to the winding surface and fixed with springs from the back.
- (c) Since there is only one single layer of magnets, for each grid location  $(\theta, \phi)$  on the winding surface, there is no reversed magnetizations or vacancies in between magnet

layers, as in the previous designs [8, 9]. This may reduce the redundancy in the usage of magnet material. To further reduce the total amount of the magnet material usage, relaxing the magnet orientation is required.

- (d) In this work, a dense mesh ( $120 \times 240$ ) has been used in the computation to improve the field design accuracy. However, this design allows for a much coarser mesh for the magnet distribution during engineering implementation. Since the outer surface  $\partial D_h$  of the permanent magnets constitutes a continuous surface, it can be re-divided into a much coarser mesh to reduce the number of magnet pieces and simplify the engineering implementation.
- (e) Although establishment of the 2D Fourier base function database needs a relatively long computational time, it only needs to be computed once. The rest part of the algorithm is rather fast.

Although we have only shown the design results for a quasi-axisymmetric stellarator, the new algorithm can be applied to any configurations. The design solution obtained with this algorithm could be a relatively good initial guess for further nonlinear optimization with more sophisticated codes. For future work, further development in the algorithm is required to relax the constraint on the orientation of the permanent magnets to reduce the total volume of the magnets and allow stay-away zones to incorporate ports. The total volume of magnets used depends on the grids of magnet distribution. Given the same grids, in principle relaxing the constraint on the magnet orientation would allow the total volume of magnets to be reduced, as it would make use of the effect of Halbach array [11]. However, if the grids are different, the result may be opposite. For example, the results of Zhu *et al* [9] shows that with the same grids, compared with the perpendicular only solution, an orientation-optimized solution uses less magnets. However, with the so-called ‘curved bricks’ grids, an orientation-optimized solution uses more magnets than the former two solutions. On the other hand, an arbitrary orientation of the magnets would dramatically increase the difficulty and cost of permanent magnet manufacturing.

The feasibility of using permanent magnets in reactor-size stellarators for fusion energy application is still debatable. One should consider the fact that the permanent magnets have to be placed outside the vacuum vessel which will be at least 1 m away from the plasma as there is a breeding blanket in between. To achieve tritium self-sufficiency, a breeding blanket of at least 1 m thick is required [21]. The field strength produced by the permanent magnets on the plasma surface is limited by the maximum achievable remanence  $B_r$  of the material, which is less than 1.59 T even at liquid nitrogen temperature for currently commercially available magnets such as Pr–Fe–B and Nd–Fe–B [22], except for some special material such as  $\text{Fe}_{16}\text{N}_2$  with  $B_r$  up to 2.9 T [23]. Although the permanent magnets are used only to compensate the normal field on the plasma surface, which is typically one order of magnitude smaller than the strong background field, it is still very challenging. However, we can use permanent magnets to compensate part of the normal field or produce part of the rotational transform, while we still use 3D modular coils instead of

the identical circular planar coils. Even though, the coil complexity can be substantially reduced, which will greatly facilitate the machine construction and cost reduction. Furthermore, higher field strength can be achieved for a reactor-size stellarator as the mechanical stresses in the coils and the support structure of the coils are reduced.

At liquid nitrogen temperature, permanent magnet materials, such as Pr–Fr–B, have a higher remanence  $B_r$  (up to 1.59 T) and intrinsic coercivity  $H_{cj}$  (larger than 7 T) [22], supposing that the permanent magnets are contained in a cryostat. We note that the demagnetization is mostly effective when the applied background magnetic field is in the opposite direction of the magnet magnetization. However, the projection of the background field in the opposite direction of the magnet magnetization is usually much smaller than the background field for most permanent magnets, especially in an  $n = 2$  quasi-axisymmetric configuration, such as the ESTELL, where the maximum ratio of the projection to the background field is only about 20%. This may imply that the magnets could maintain magnetization in a relatively strong background field. More study is required to clarify this point.

The magnetic field strength produced by permanent magnets appears to be insufficient for a self-sustained fusion reactor. However, it may be sufficient for a fusion neutron source with a neutron wall loading of  $\leq 0.2 \text{ MW m}^{-2}$ , corresponding to a neutron flux rate of  $\leq 9 \times 10^{16} \text{ m}^{-2} \text{ s}^{-1}$ , which only needs a shielding blanket of  $\leq 0.3 \text{ m}$  thick [24]. Furthermore, a big advantage of using permanent magnets relative to copper coils is steady state operation without energy consumption. Compared with superconducting magnets, permanent magnets are much inexpensive. Stellarators with permanent magnets and simple superconducting coils may thus open up a promising new avenue for the development of less-expensive steady-state fusion neutron sources.

## Acknowledgments

We would like to acknowledge Michael Drevlak for the ESTELL equilibrium and the helpful communications with Caixiang Zhu, Haifeng Liu, Samuel Lazerson and Jie Huang. This work was supported by the National Magnetic Confinement Fusion Energy R & D Program of China under Grant No. 2019YFE03030000, the National Natural Science Foundation of China under Grant No. U19A20113, the Key Research Program of Frontier Sciences, CAS under Grant No. QYZDB-SSW-SLH001, the CASHIPS Director's Fund under Grant No. BJPY2019A01 and the K.C. Wong Education Foundation.

## ORCID iDs

G.S. Xu  <https://orcid.org/0000-0001-8495-8678>

## References

- [1] Xu Y. 2016 A general comparison between tokamak and stellarator plasmas *Matter Radiat. Extremes* **1** 192–200
- [2] Canik J.M. et al 2007 Experimental demonstration of improved neoclassical transport with quasihelical symmetry *Phys. Rev. Lett.* **98** 085002
- [3] Bosch H.S. et al 2013 Technical challenges in the construction of the steady-state stellarator Wendelstein 7-X *Nucl. Fusion* **53** 126001
- [4] Strykowski R.L., Brown T., Chrzanowski J., Cole M., Heitzenroeder P., Neilson G.H., Rej D. and Viola M. 2009 Engineering cost & schedule lessons learned on NCSX 23rd *IEEE/NPSS Symposium on Fusion Engineering* (San Diego, CA, 8–10 August 1995) pp 1–4 (<https://ieeexplore.ieee.org/abstract/document/5226449>)
- [5] Najmabadi F. and Raffray A.R. 2008 The ARIES-CS compact stellarator fusion power plant *Fusion Sci. Technol.* **54** 655–72
- [6] Helander P., Drevlak M., Zarnstorff M. and Cowley S.C. 2020 Stellarators with permanent magnets *Phys. Rev. Lett.* **124** 095001
- [7] Matsuura Y. 2006 Recent development of Nd–Fe–B sintered magnets and their applications *J. Magn. Magn. Mater.* **303** 344–7
- [8] Zhu C., Zarnstorff M., Gates D. and Brooks A. 2020 Designing stellarators using perpendicular permanent magnets *Nucl. Fusion* **60** 076016
- [9] Zhu C., Hammond K., Brown T., Gates D., Zarnstorff M., Corrigan K., Sibilia M. and Feibush E. 2020 Topology optimization of permanent magnets for stellarators *Nucl. Fusion* **60** 106002
- [10] Rozvany G.I.N. and Zhou M. 1991 The COC algorithm, part I: cross-section optimization or sizing *Comput. Methods Appl. Mech. Eng.* **89** 281–308
- [11] Halbach K. 1980 Design of permanent multipole magnets with oriented rare earth cobalt material *Nucl. Instrum. Methods* **169** 1–10
- [12] Hammond K.C., Zhu C., Brown T., Corrigan K., Gates D.A. and Sibilia M. 2020 Geometric concepts for stellarator permanent magnet arrays *Nucl. Fusion* **60** 106010
- [13] Drevlak M., Brochard F., Helander P., Kisslinger J., Mikhailov M., Nührenberg C., Nührenberg J. and Turkin Y. 2013 ESTELL: a quasi-toroidally symmetric stellarator *Contrib. Plasma Phys.* **53** 459
- [14] Nührenberg J., Lotz W. and Gori S. 1994 *Theory of Fusion Plasmas* (Bologna: Editrice Compositori) p 3
- [15] Boozer A.H. 1995 Quasi-helical symmetry in stellarators *Plasma Phys. Control. Fusion* **37** A103
- [16] Helander P. 2014 Theory of plasma confinement in non-axisymmetric magnetic fields *Rep. Prog. Phys.* **77** 087001
- [17] Jackson J.D. 2007 *Classical Electrodynamics[M]* (New York: Wiley)
- [18] Merkel P. 1987 Solution of stellarator boundary value problems with external currents *Nucl. Fusion* **27** 867–71
- [19] Wang G., Yimin W. and Qiao S. 2004 Equation solving generalized inverses *Generalized Inverses: Theory and Computations* (Beijing: Science Press) p 6
- [20] Sarafyan D. 1972 Improved sixth-order Runge–Kutta formulas and approximate continuous solution of ordinary differential equations *J. Math. Anal. Appl.* **40** 436–45
- [21] El-Guebaly L. et al 2008 Designing aries-CS compact radial build and nuclear system: neutronics, shielding, and activation *Fusion Sci. Technol.* **54** 747–70
- [22] He Y.-Z., Wu H.-P. and Zou Z.-Q. 2014 Magnetic properties of bulk polycrystalline  $\text{Pr}_{1-x}\text{Nd}_x$  ( $x = 0, 0.8$ )FeB permanent magnets *Chin. Phys. B* **23** 047501
- [23] Wang J.-P. 2020 Environment-friendly bulk  $\text{Fe}_{16}\text{N}_2$  permanent magnet: review and prospective *J. Magn. Magn. Mater.* **497** 165962
- [24] Liu H., Abdou M.A., Reed R.J., Ying A. and Youssef M.Z. 2010 Neutronics assessment of the shielding and breeding requirements for FNSF (standard aspect ratio) *Fusion Eng. Des.* **85** 1296–300